LRP 540/96 February 1996

SYMPLECTIC FINITE ELEMENT SCHEME: APPLICATION TO A DRIVEN PROBLEM WITH A REGULAR SINGULARITY

A. Pletzer

Submitted to
Computer Physics Communications

Symplectic finite element scheme: Application to a driven problem with a regular singularity

A. Pletzer

Centre de Recherches en Physique des Plasmas
Association Euratom – Confédération Suisse
Ecole Polytechnique Fédérale de Lausanne
CH-1007 Lausanne, Switzerland
E-mail: alexandre.pletzer@crpp.epfl.ch

Abstract

A new finite element (FE) scheme, based on the decomposition of a second order differential equation into a set of first order symplectic (Hamiltonian) equations, is presented and tested on a one-dimensional, driven Sturm-Liouville problem. Error analysis shows improved cubic convergence in the energy norm for piecewise linear "tent" elements, as compared to quadratic convergence for the standard and hybrid FE methods. The convergence deteriorates in the presence of a regular singular point, but can be recovered by appropriate mesh node packing. Optimal mesh packing exponents are derived to ensure cubic (respectively quadratic) convergence with minimal numerical error. A further suppression of the numerical error by a factor proportional to the square of the leading exponent of the singular solution, is achieved for a model problem based on determining the nonideal magnetohydrodynamic stability of a fusion plasma.

PACS: 02.70.Dh, 52.30.Jb

keywords: Finite elements, Hamiltonian, symplectic, resistive MHD stability

1 Introduction

The purpose of the present paper is to explore the numerical gain in accuracy that can be obtained by decomposing a second order ordinary differential equation into a system of first order equations. Such a decomposition is generally required to make an initial value problem numerically tractable, but is not common in the case of boundary value problems. There are reasons, however, which contribute to make this decomposition an attractive scheme. Firstly, it introduces additional dependent variables, which increases the dimension of the Sobolev space from which trial functions are drawn to minimize the action

functional (at the heart of the finite element method). This leads to higher accuracy. Secondly, the decomposition can ensure that the dependent variables obtained by decomposition are determined with the same accuracy as the unknown solutions. This may be required in particular physical problems.

The advantage of splitting a higher order equation disappears if the decomposition does not preserve properties such as self-adjointness. Not all decompositions are therefore appropriate. In Section 2 we develop the formalism of Hamiltonian systems, that is an infinite class of equivalent Hermitian systems. Any such system can be generated from another using symplectic (canonical) transformations. (For a good introduction to other properties of such systems, see Appendix C of Ref. [1]).

In Section 3 we estimate the convergence rate of the error for the symplectic finite element method. Two choices of finite elements expansions are adopted for the Galerkin-Ritz approximation of the conjugate "momentum" solution: the piecewise constant and piecewise linear ('tent') elements. These choices have distinct convergence features. In particular, the deterioration of the convergence rate in the presence of a regular singular point gives rise to different mesh packing criteria.

To test the usefulness of the symplectic FE scheme, a singular problem of asymptotic matching which arises in the context of resistive magnetohydrodynamic instabilities in a plasma, is constructed in Section 4. Convergence rates in energy norm are computed in Section 5 for this exact case, and compared with theoretical predictions.

2 Hamiltonian Decomposition

Consider the driven Sturm-Liouville equation,

$$Ly(x) \equiv [f(x)y'(x)]' - g(x)y(x) = r_1(x) - r_2'(x) \tag{1}$$

subject to the boundary conditions

$$\begin{aligned} y'(0) + \beta_0 y(0) &= \gamma_0 \\ y'(1) + \beta_1 y(1) &= \gamma_1 \end{aligned} \tag{2}$$

at $x = 0$, and $x = 1$ respectively.

A Lagrangian density,

$$\mathcal{L} = \tfrac{1}{2} f y'^2 + \tfrac{1}{2} g y^2 + r_1 y + r_2 y', \tag{3}$$

can be constructed such that (1) is the Euler-Lagrange equation,

$$\left(\frac{\partial \mathcal{L}}{\partial y'}\right)' - \frac{\partial \mathcal{L}}{\partial y} = 0, \tag{4}$$

which extremizes the action

$$\mathcal{S} \equiv \int dx \mathcal{L}; \tag{5}$$

i.e., $\delta S = 0$ for arbitrary variations δy that vanish at the end-points.

A conjugate momentum to y can be defined,

$$p \equiv \frac{\partial \mathcal{L}}{\partial y'} = f y' + r_2, \tag{6}$$

as well as a Hamiltonian density,

$$\mathcal{H} \equiv p y' - \mathcal{L} = -\tfrac{1}{2} f y'^2 - \tfrac{1}{2} g y^2 - r_1 y. \tag{7}$$

Equation (1) can then be rewritten,

$$\begin{aligned} -p' &= \partial \mathcal{H}/\partial y = -gy - r_1 \\ y' &= \partial \mathcal{H}/\partial p = f^{-1}(p - r_2) \end{aligned} \tag{8}$$

as a system of two first order equations. A more compact notation for (8) is

$$\mathbf{E} \cdot \mathbf{y}' - \mathbf{H} \cdot \mathbf{y} = \mathbf{s}, \tag{9}$$

where

$$\mathbf{E} \equiv \begin{pmatrix} 0 & -1 \\ 1 & 0 \end{pmatrix}, \quad \mathbf{y} \equiv \begin{pmatrix} y \\ p \end{pmatrix}, \quad \mathbf{H} \equiv \begin{pmatrix} -g & 0 \\ 0 & f^{-1} \end{pmatrix}, \tag{10}$$

and

$$\mathbf{s} \equiv \begin{pmatrix} -r_1 \\ -f^{-1}r_2 \end{pmatrix}. \tag{11}$$

Such a system is called *Hamiltonian.*

All transformations $\mathbf{U}$

$$\mathbf{y} \rightarrow \bar{\mathbf{y}} = \mathbf{U}\cdot\mathbf{y} \tag{12}$$

which conserve the Hamiltonian form (9) are called *canonical.* Since the action $\mathcal{S} = \int dx \mathbf{y}\cdot(\mathbf{E}\cdot\mathbf{y}' - \mathbf{H}\cdot\mathbf{y} - \mathbf{s})$ is an invariant,

$$\bar{\mathcal{S}} \equiv \int dx(\mathbf{U}\cdot\mathbf{y})\cdot(\mathbf{E}\cdot\mathbf{U}\cdot\mathbf{y}' - [\mathbf{H}\cdot\mathbf{U} - \mathbf{E}\cdot\mathbf{U}']\cdot\mathbf{y} - \mathbf{s}) = \mathcal{S}, \tag{13}$$

one immediately finds that $\mathbf{U}$ must satisfy the condition

$$\mathbf{U}^T\cdot\mathbf{E}\cdot\mathbf{U} = \text{const}\mathbf{E}, \tag{14}$$

that is, $\mathbf{U}$ is a *symplectic* matrix [2].

We regard all Hamiltonian systems generated by $\mathbf{U}$ satisfying (14) as equivalent forms to the initial problem (1). Take for instance the symplectic transformation

$$p \rightarrow \bar{p} = p + ey, \tag{15}$$

that redefines the conjugate momentum but leaves the solution unchanged; that is,

$$\mathbf{U} = \begin{pmatrix} 1 & 0 \\ e(x) & 1 \end{pmatrix}. \tag{16}$$

The transformed Hamiltonian matrix and source term map into

$$\mathbf{H} \rightarrow \begin{pmatrix} f^{-1}e^2 - \bar{g} & -f^{-1}e \\ -f^{-1}e & f^{-1} \end{pmatrix} \quad \text{and} \quad \mathbf{s} \rightarrow \begin{pmatrix} f^{-1}er_2 - r_1 \\ -f^{-1}r_2 \end{pmatrix}, \tag{17}$$

where $\bar{g} = g + e'$. These are the most general forms of $\mathbf{H}$ and $\mathbf{s}$ for a self-adjoint second order differential equation with a source term, which conserve the self-adjointness of the system ($\mathbf{H} = \mathbf{H}^T$). This property can then be exploited numerically.

The concepts of conjugate momenta and Hamiltonian density are very general; they can be defined for all equations. The definitions (6) and (7), however, only apply to the Sturm-Liouville Eq. (1). These definitions would require revision to account for higher order derivatives (equations of order exceeding two) and the fact that the adjoint solution $\tilde{y}$ may differ from y (as in the case of non-selfadjoint equations). A pathological situation is encountered when p is linearly dependent on y as in the case of a first order equation. Of course we must discard such degenerate systems (see e.g. the case of the diffusion equation treated in Ref.[3]).

3 Error Estimates

Multiplying (9) on the left by the row vector $\frac{1}{2}(u \;\; p_u)$ and integrating over the domain $(0,1)$, we obtain the weak form

$$W_H(\mathbf{u},\mathbf{y}) = -\tfrac{1}{2}\int_0^1 dx \left(u r_1 + p_u f^{-1} r_2\right) \tag{18}$$

of (8), where

$$W_H(\mathbf{u},\mathbf{v}) \equiv \tfrac{1}{2}\int_0^1 dx \left(-p_u f^{-1} p_v + u' p_v + p_u v' + u g v\right) - \tfrac{1}{2}\left[u p_v\right]_0^1 \tag{19}$$

is the energy inner product, and p_u and p_v are the conjugate variables to u and v, respectively. Approximating the solution $\mathbf{y}$ by an expansion (Ritz approximation)

$$\tilde{\mathbf{y}} \equiv \sum_{k=1}^{2}\sum_{i=1}^{M} c_i^{(k)} \mathbf{e}_i^{(k)}(x) \tag{20}$$

in finite elements $\mathbf{e}_i^{(k)}$,

$$\mathbf{e}_i^{(1)} = \begin{pmatrix} e_i^{(1)}(x) \\ 0 \end{pmatrix} \quad \text{and} \quad \mathbf{e}_i^{(2)} = \begin{pmatrix} 0 \\ e_i^{(2)}(x) \end{pmatrix}, \tag{21}$$

we find the linear system of equations

$$\sum_{k=1}^{2}\sum_{i=1}^{M} W_{\rm H}(\mathbf{e}_{\rm j}^{(l)}, \mathbf{e}_{\rm i}^{(k)}) c_{\rm i}^{(k)} = \frac{1}{2}\int_0^1 dx \mathbf{e}_{\rm j}^{(l)} \cdot \mathbf{s} \quad (l = 1,2 \text{ and } j = 1, 2 \cdots M). \tag{22}$$

In general, the basis functions $e_{\rm i}^{(1)}(x)$ and $e_{\rm i}^{(2)}(x)$ need not be identical. Noting that no derivatives of $e_{\rm i}^{(2)}(x)$ appear in (18) and (19), $e_{\rm i}^{(2)}(x)$ may be taken as piecewise constant, whereas the $e_{\rm i}^{(1)}(x)$ must, at least, be piecewise linear. Such a choice of hybrid elements will be treated in details in Section 3.1.

Note also from the weak form (18) that the error $\epsilon \equiv \tilde{\mathbf{y}} - \mathbf{y}$ is orthogonal to the space spanned by the basis functions $\mathbf{e}_{\rm i}^{(k)}$: i.e.,

$$W_{\rm H}(\mathbf{e}_{\rm j}^{(l)}, \epsilon) = 0 \tag{23}$$

and therefore the error in energy norm

$$W_{\rm H}(\tilde{\mathbf{y}}, \tilde{\mathbf{y}}) - W_{\rm H}(\mathbf{y}, \mathbf{y}) = W_{\rm H}(\epsilon, \epsilon) \tag{24}$$

converges quadratically in ϵ. Such a property also exists for the ordinary FE method.

3.1 Symplectic hybrid elements (SHE)

To proceed further we adopt the hybrid basis elements:

$$e_{\rm i}^{(1)}(x) = \begin{cases} 0, & x < x_{\rm i-1} \text{ or } x > x_{\rm i+1} \\ (x - x_{\rm i-1})/(x_{\rm i} - x_{\rm i-1}), & x_{\rm i-1} \le x \le x_{\rm i} \\ (x_{\rm i+1} - x)/(x_{\rm i+1} - x_{\rm i}), & x_{\rm i} \le x \le x_{\rm i+1} \end{cases} \tag{25}$$

for y, and

$$e_{\rm i}^{(1)}(x) = \begin{cases} 0, & x < x_{\rm i} \text{ or } x > x_{\rm i+1} \\ 1, & \text{elsewhere} \end{cases} \tag{26}$$

for p. A similar choice of finite elements has been made in Ref.[4].

Assuming that the approximate solution $\tilde{\mathbf{y}}$ approaches pointwise the exact solution $\mathbf{y}$ as $M \to \infty$, we make the following ansatz for the error estimates [5]:

$$\left.\begin{array}{l} \epsilon \propto \frac{1}{2} y_{\mathrm{i}}'' h_{\mathrm{i}}^2 \ , \ \epsilon' \propto y_{\mathrm{i}}'' h_{\mathrm{i}} \\ \text{and} \qquad\qquad p_\epsilon \propto p_{\mathrm{i}}' h_{\mathrm{i}} \end{array}\right\} \quad \text{for } x_{\mathrm{i}} \le x \le x_{\mathrm{i}+1}, \tag{27}$$

at lowest order in $h_{\mathrm{i}} \equiv x_{\mathrm{i}+1} - x_{\mathrm{i}}$. Here, y_{i}'' and p_{i}' are understood to be the maximal values of $y''(x)$ and $p'(x)$, respectively, within the node interval $(x_{\mathrm{i}}, x_{\mathrm{i}+1})$. This allows us to write

$$W_{\mathrm{H}}(\epsilon, \epsilon) \propto \sum_{\mathrm{i}=1}^{M-1} \frac{1}{2} \int_{x_{\mathrm{i}}}^{x_{\mathrm{i}+1}} dx \left\{ -\left(f^{-1}\right)_{\mathrm{i}} p_{\mathrm{i}}'^2 h_{\mathrm{i}}^2 + y_{\mathrm{i}}'' p_{\mathrm{i}}' h_{\mathrm{i}}^2 + \frac{1}{4} g_{\mathrm{i}} y_{\mathrm{i}}''^2 h_{\mathrm{i}}^4 \right\}, \tag{28}$$

plus some higher order terms in h_{i}. For bounded $|y_{\mathrm{i}}''| \sim |p_{\mathrm{i}}'| < \infty$, it is clear that the first two terms dominate at large $M \sim 1/h$ and that they produce a convergence rate in M^{-2}.

The picture is quite different in the singular case, i.e. when y_{i}'' and p_{i}' are potentially unbounded. To be more specific, let us assume a regular singular point at $x = 0$:

$$f(x) \sim x^2, \ \ g \sim g_0, \ \ y \sim C x^\alpha \ \ \text{and} \, p \sim C\alpha x^{\alpha+1}, \ \ \text{as } x \to 0, \tag{29}$$

the behaviour of p being in agreement with (6) and α assumed $\neq 0$ or 1. Anticipating accuracy problems of the solution in the vicinity of $x = 0$, we allow the mesh nodes x_{i} to be distributed according to

$$x_{\mathrm{i}} = (i/M)^\gamma \equiv t^\gamma \tag{30}$$

with the mesh packing exponent $\gamma \ge 1$ controlling the density of nodes. The choice of a power law for the mesh packing is motivated by the singular behaviour of the solution. (A different ansatz would be required in the case of an essential singularity.)

Taking the limit of $M \to \infty$, we have

$$\begin{aligned} \textstyle\sum_{\mathrm{i}} &\to M \int_{0+}^{1} dt \\ 1/M &\to dt \\ h_{\mathrm{i}} &\to dx = \gamma t^{\gamma-1}/M \end{aligned} \tag{31}$$

and inserting these relations in (28) we obtain

$$W_{\mathrm{H}}(\epsilon,\epsilon) \sim \tfrac{1}{2}C^2\alpha^2\gamma^3 \left[\frac{A_{\mathrm{h}}}{(2\alpha+1)\gamma-2} \left(M^{-2} - M^{-(2\alpha+1)\gamma}\right) + \frac{\gamma^2 B_{\mathrm{h}}}{(2\alpha+1)\gamma-4} \left(M^{-4} - M^{-(2\alpha+1)\gamma}\right) \right] \tag{32}$$

at leading orders in $1/M$, where A_{h} and B_{h} are constants which depend on the coefficients of proportionality in (27).

It is immediately apparent that the energy error $W_{\mathrm{H}}(\epsilon,\epsilon)$ reaches a maximum convergence rate in M^{-2} provided

$$\gamma > \frac{2}{2\alpha+1}. \tag{33}$$

Note that the poles in (32) are only apparent since we have, for instance,

$$\lim_{\gamma \to 2/(2\alpha+1)} \frac{M^{-2} - M^{-(2\alpha+1)\gamma}}{(2\alpha+1)\gamma-2} = M^{-2}\ln M, \tag{34}$$

which yields

$$W_{\mathrm{H}}(\epsilon,\epsilon) \sim \tfrac{1}{2}C^2\alpha^2\gamma^3 \left[A_{\mathrm{h}}M^{-2}\ln M + \tfrac{1}{2}\gamma^2 B_{\mathrm{h}}M^{-2}\right] \quad \text{as } \gamma \to 2/(2\alpha+1). \tag{35}$$

In this limit, the density of energy error (35) spreads evenly over the $(0,1)$ domain. If however (33) were not satisfied, then the energy error density would peak in the vicinity of the singularity and the contribution to $W_{\mathrm{H}}(\epsilon,\epsilon)$ arising from the first node would dominate over the remaining integral. This would result in a reduction of the convergence rate,

$$W_{\mathrm{H}}(\epsilon,\epsilon) \propto M^{-\gamma(2\alpha+1)} \tag{36}$$

with the coefficient of proportionality depending on δ, the small distance which defines the position of the first element away from the singular point. Note also that the error in energy norm is seen in (32) to be $\propto \gamma^2$ for large γ, indicating that the scaling $\gamma = 2/(2\alpha+1)$ is optimal, in the sense of providing the highest convergence rate for the smallest error.

3.2 Symplectic tent elements (STE)

Since the error for hybrid elements was dominated by the Ritz representation of the conjugate momentum, the choice of tent elements (25) for both expansions y and p provides the hope to increase further the convergence rate. By selecting smoother basis functions, a price must however be paid; the number of upper diagonals in the sparse linear system (22) resulting from the overlap of neighbouring basis elements increases from two to three.

The derivation of the error estimate is in every point similar to the one in Section 3.2, with the difference now that

$$p_\epsilon \propto \tfrac{1}{2} p_i'' h_i^2, \tag{37}$$

which suggest higher order error. Introducing (37) with the error bounds for ϵ and ϵ' in (19), we find the expression

$$\begin{aligned} W_{\mathrm{H}}(\epsilon,\epsilon) \sim \tfrac{1}{2} C^2 \alpha^2 \gamma^4 \Bigg[& \frac{A_t}{(2\alpha+1)\gamma - 3} \left(M^{-3} - M^{-(2\alpha+1)\gamma} \right) \\ & + \frac{\gamma B_t}{(2\alpha+1)\gamma - 4} \left(M^{-4} - M^{-(2\alpha+1)\gamma} \right) \Bigg], \end{aligned} \tag{38}$$

where A_t and B_t are, again, constants which depend on the ϵ, ϵ' and p_ϵ estimates.

The maximum convergence rate is found to be in M^{-3}, provided

$$\gamma \geq \frac{3}{2\alpha+1}, \tag{39}$$

with the limit,

$$W_{\mathrm{H}}(\epsilon,\epsilon) \sim \tfrac{1}{2} C^2 \alpha^2 \gamma^4 \left[A_t M^{-3} \ln M + \gamma B_t M^{-3} \right] \quad \text{as } \gamma \to 3/(2\alpha+1) \tag{40}$$

well defined. Note that condition (39) is more restrictive than (33). For (39) not satisfied, the convergence rate reduction is given by (36) in this case too. Mesh packing with γ in excess of (39) should be avoided, for the energy error increases proportionally to γ^3 at large γ's. The convergence rates of the hybrid and tent element schemes are summarized in Fig. 1.

4 Test Problem

The following problem arises in studying resistive (so called "tearing") modes which develop within the framework of the resistive magnetohydrodynamic (MHD) plasma model. It is known that Eq.(1) with $r_1 = r_2 = 0$ approximates the equation [6] governing the plasma displacement field ξ in the vicinity of a singular surface at $x = 0$ where

$$f(x) \sim x^2 + f_1 x^3 + \cdots \text{ and } g(x) = g_0 + g_1 x + g_2 x^2 + \cdots . \tag{41}$$

The singularity at $x = 0$ gives rise to two independent solutions,

$$\begin{aligned} \xi^{(\mathrm{b})} &= x^{-\frac{1}{2}-\mu}\{\xi_0^{(\mathrm{b})} + \xi_1^{(\mathrm{b})} x + \xi_2^{(\mathrm{b})} x^2 + \cdots\} \\ \xi^{(\mathrm{s})} &= x^{-\frac{1}{2}+\mu}\{\xi_0^{(\mathrm{s})} + \xi_1^{(\mathrm{s})} x + \xi_2^{(\mathrm{s})} x^2 + \cdots\} \end{aligned} , \tag{42}$$

with superscript (b, s) corresponding to the big and small leading exponents $\alpha = -1/2 \pm \mu$, respectively, where

$$\mu \equiv \sqrt{\tfrac{1}{4} + g_0} \tag{43}$$

is assumed positive and real.

The quantity of interest is the ratio $\Delta' \equiv \xi_0^{(\mathrm{s})}/\xi_0^{(\mathrm{b})}$ which drives the 'tearing' mode unstable when positive. (To be more precise, the ratio is computed taking the jump of small solution to odd large solution but the parities have no incidence on the difficulty of computing Δ' so that we are entitled to focus here on the one-sided, $x > 0$ problem.) As $x \to 0$, we have

$$\xi \sim \text{ const}(\xi^{(\mathrm{b})} + \Delta' \xi^{(\mathrm{s})}) \tag{44}$$

and Δ' is given by the jump of the bilinear concomitant [7,8] of

$$\hat{\xi} \sim \xi^{(\mathrm{b})} \text{ and } \check{\xi} \sim \Delta' \xi^{(\mathrm{s})}, \tag{45}$$

which in turn can be expressed

$$\mu \Delta' = W(\check{\xi}, \check{\xi}) + \tfrac{1}{2} \int_0^1 dx \hat{\xi}(L\hat{\xi}) \tag{46}$$

in terms of the functional

$$W(u,v) \equiv \tfrac{1}{2}\int_0^1 dx\,(u'fv' + ugv) - \tfrac{1}{2}\,[ufv']_0^1, \tag{47}$$

which represents the "ideal" energy of the plasma. In real situation, $W(u,v)$ (which differs from $W_{\rm H}$) is often positive definite and when this is case, the error in computing Δ' from (46) gives a systematic negative error.

We take $\hat{\xi}$ to be a prescribed function which approximates $\xi^{(b)}$ to an accuracy which is recessive to the small solution $\xi^{(s)}$. Otherwise, $\hat{\xi}$ is arbitrary. The unknown solution is called $\check{\xi}$ and is obtained by solving

$$L\check{\xi} = -L\hat{\xi} \tag{48}$$

where $-L\hat{\xi}$ acts as a source term. We require $\check{\xi}$ to have the $\xi^{(s)}$ behaviour as $x \to 0$ and to satisfy homogeneous Dirichlet boundary conditions at $x = 1$. (In fact, the numerical scheme automatically selects the asymptotic solution with $\xi^{(s)}$ behaviour by assuming finite W, as long as $-L\hat{\xi}$ is compatible with $\hat{\xi} \sim \xi^{(b)}$.)

Because the second term on the right hand side of (46) is prescribed and therefore independent of M, the error in Δ' arises entirely from computing $W(\check{\xi},\check{\xi})$.

A similar expression to (46) can be obtained for the Hamiltonian system by replacing W by $W_{\rm H}$ and $\hat{\xi}(L\hat{\xi})$ by $\hat{\mathbf{y}}\cdot(\mathbf{E}\cdot\hat{\mathbf{y}}' - \mathbf{H}\cdot\hat{\mathbf{y}})$.

5 Results

An exact test case [9] is constructed by taking

$$f(x) = x^2 \text{ and } g(x) = g_0 + x^2. \tag{49}$$

The small and big solutions (for $g_0 > -1/4$) are $\xi^{(s)} = 2^\mu\Gamma(1+\mu)x^\mu \mathrm{I}_\mu(x)$ and $\xi^{(b)} = 2^{-\mu}\Gamma(1-\mu)x^{-\mu}\mathrm{I}_{-\mu}(x)$, respectively, where $\mathrm{I}_{\pm\mu}$ are modified Bessel functions [10]. By requiring $\xi = \xi^{(s)} + \Delta'\xi^{(b)}$ to vanish at $x = 1$, we get

$$\Delta' = \left(\tfrac{1}{2}\right)^{2\mu}\frac{\Gamma(-\mu)\mathrm{I}_{-\mu}(1)}{\Gamma(\mu)\mathrm{I}_\mu(1)}. \tag{50}$$

Note that since Δ' can be identified with C in (29), we expect the relative error in Δ' to be proportional to Δ' from Eqs. (35)–(38) and (46). In the case of a plasma at the marginal ideal stability point ($|\Delta'| \to \infty$), the relative numerical error would formally be infinite.

In the following, we will treat the three cases summarized in Table (51)

g_0	μ	α	Δ'
-5/36	1/3	-1/6	-1.1721654155
0	1/2	0	-1.3130352855
7/36	2/3	1/6	-1.5752523228

(51)

We first focus on the case $g_0 = -5/36$, for which the solution $|\check{\xi}| \to \infty$ is unbounded as $x \to 0$. This case is numerically the most demanding, for μ is small so that a mesh packing exponent $\gamma = 3$ is required for the FE and SHE schemes, respectively $\gamma = 4.5$ for the STE scheme, in order to achieve convergence in M^{-2}.

Figure 2 shows the relative error of the SHE scheme versus the number of mesh nodes $M = 2, 3, 4 \cdots 100$. The picture confirms the predictions of the convergence rate of the SHE scheme versus the mesh packing exponent γ: that is the error is estimated graphically to be $\propto M^{-0.7}$ for a linear mesh, $\propto M^{-1.2}$ for $\gamma = 1.5$, $\propto M^{-2.1}$ for $\gamma = 3$ and $\propto M^{-2.0}$ for $\gamma = 4.5$. Increasing γ beyond $1/\mu$ does not improve the convergence rate but rather increases the error by a factor approximately $(\gamma\mu)^3 = 3.4$, in good agreement with the numerical results.

A similar study has be performed for the SHE scheme in Fig. 3. The convergence rate in $M^{-1.0}$ for $\gamma = 1.5$ agrees well with predictions given in Section 3.2. The most striking features of the STE error at $\gamma = 4.5$ are the numerous spikes in the convergence behaviour, which are exacerbated when both M and γ increase.

The are two reasons which explain the rough behaviour of the error convergence. First, the attempt by the numerical scheme to extremize the indefinite functional $W_{\mathrm{H}}(\epsilon, \epsilon)$ by switching its sign. This is shown in Fig. 7 for the case $g_0 = 0$ (corresponding to a pressureless plasma), where the points yielding a negative error are made distinct from those having $W_{\mathrm{H}}(\epsilon, \epsilon) > 0$; most of the peak points in the STE error convergence behaviour coincide with $W_{\mathrm{H}}(\epsilon, \epsilon)$ changing sign. The indefiniteness of W_{H} can also be observed for the SHE scheme, but is inhibited at large M's due to the positive definite part $\frac{1}{2}\int dx(-f^{-1}p_\epsilon^2 + 2\epsilon' p_\epsilon)$ of W_{H} which dominates over $\frac{1}{2}\int dx g\epsilon^2$. To see this, let

us assume y and $p \propto \exp(\mathrm{i}kx)$ so that the discretized form of dy/dx reads as

$$\delta_{\mathrm{h}}^{(\mathrm{SHE})} y(x_{\mathrm{i}}) \equiv \frac{y(x_{\mathrm{i+1}}) - y(x_{\mathrm{i}})}{h} = \frac{2\mathrm{i}}{h} \exp(\mathrm{i}kh/2) \sin(kh/2) \tag{52}$$

for the SHE scheme, whereas

$$\delta_{\mathrm{h}}^{(\mathrm{STE})} y(x_{\mathrm{i}}) \equiv \frac{y(x_{\mathrm{i+1}}) - y(x_{\mathrm{i-1}})}{2h} = \frac{\mathrm{i}}{h} \sin(kh) \tag{53}$$

for the STE scheme, where $h \equiv x_{\mathrm{i+1}} - x_{\mathrm{i}} = x_{\mathrm{i}} - x_{\mathrm{i-1}}$ (for a linear mesh). Both discretization schemes yield $\delta_{\mathrm{h}} \rightarrow d/dx = \mathrm{i}k$ in the limit of $h \rightarrow 0$ and k finite; they are good approximations in the moderate k range. The behaviour of the SHE and STE discretizations, however, differ significantly as k approaches $k_{\mathrm{max}} = \pi/h$, the value corresponding to the shortest wavelength that can be described considering the mesh resolution; $\delta_{\mathrm{h}}^{(\mathrm{SHE})}$ increases to attain $-2/h$ whereas $\delta_{\mathrm{h}}^{(\mathrm{STE})}$ decreases to vanish at $k = k_{\mathrm{max}}$.

The second reason for the rough convergence behaviour is that the SHE solution is "stiffer" than the STE since small wavelength oscillations have a larger W_{H} energy. The fact that $\delta_{\mathrm{h}}^{(\mathrm{STE})} \rightarrow 0$ in this limit is reflected by the "odd-even" instability of Fig. 5 as well as the emergence of the spurious eigenvalue shown in Fig. 6 which tends to zero proportionally to $h \rightarrow 0$. This phenomenon is well known to arise in the presence of numerical pollution [11,12]. Interestingly, the polluted STE solution appears more accurate than the SHE solution in the vicinity of the regular singularity $x = 0$.

The case $g_0 = 7/36$ is more interesting from a physical viewpoint, for the quantity g_0 is generally positive in a tokamak due to favourable magnetic field line curvature. We get $\check{\xi} \rightarrow 0$ which remains bounded as $x \rightarrow 0$. A mesh packing exponent γ of 1.5 is sufficient to ensure convergence in M^{-2} for the SHE scheme, and $\gamma = 2.25$ for the STE scheme, as shown in Fig. 7. Note that the SHE scheme reduces the error of the FE scheme by a factor $30-40$ which is roughly equal to α^2. This gain is attributed to the Hamiltonian decomposition for which $p_{\mathrm{i}}' \propto \alpha y_{\mathrm{i}}''$ in (28). The STE scheme yields a further improvement of accuracy by approximately one order of magnitude.

6 Conclusions

The advantages in accuracy and convergence properties, of the Hamiltonian finite element schemes based on hybrid (SHE) and tent (STE) elements over the usual finite element scheme have been expounded, without resorting to

higher order (e.g. cubic) elements which in turn would require higher order quadrature schemes. In some problems, the physical significance attached to the conjugate variable also contributes to render the Hamiltonian scheme attractive. In the problem treated in Section 4, the conjugate variable to the normal displacement represents the total of plasma and magnetic pressure perturbation. The Hamiltonian decomposition is also useful to unveil properties of the equation. In Ref. [13] for instance, the Hamiltonian decomposition of the MHD operator was presumably used unconsciously to solve the issue about the existence of continua in the spectrum.

The relation between the mesh packing and the convergence behaviour has been clarified. The STE scheme has the strongest maximal convergence rate at the expense of a "wiggled" convergence behaviour, which is attributed to both numerical pollution and to the indefiniteness of the W_{H} energy. The incidence of numerical pollution on the behaviour of the solutions remains weak, with oscillating amplitudes averaging less than 2% of the smooth part of the solution. The accuracy of the polluted STE solution appears more accurate than the unpolluted SHE solution near the regular singular point.

The SHE scheme, on the other hand, possesses the same convergence rate as the standard finite element method (FE) with, however, an accuracy which improves by a magnitude $\sim \alpha^2$ with respect to the FE scheme. For the tearing mode stability problem, the small solution exponent α scales with the pressure gradient at the singular surface and is typically of the order of 0.01. The accuracy gain is thus substantial.

It is expected that one could avoid expensive convergence studies and extrapolations to infinite M by using the STE scheme, which requires a modest number of mesh nodes (about 10) to reach a 1% accuracy, as compared to about 100 mesh nodes required by the FE method. This point could turn out to be crucial for the resistive stability code PEST [14] when working near the ideal marginal stability point, which is shown in this paper to lead to high inaccuracy.

Acknowledgement

This work was partly supported by the Swiss National Fund Foundation.

References

[1] A. H. Glasser, C. C. Jardin, and G. Tesauro, Phys. Fluids **27**, 1225 (1984).

[2] H. Goldstein, *Classical Mechanics* (Addisson-Wesley, London, 1980).

[3] P. M. Morse and H. Feshbach, in *Methods of Theoretical Physics* (MacGraw-Hill, New York, 1953), Chap. 3.

[4] K. Appert, D. Berger, R. Gruber, and J. Rappaz, J. Comput. Phys. **18**, 284 (1975).

[5] K. W. Morton, in *Finite Elements in Physics*, edited by R. Gruber (North-Holland, Amsterdam, 1987), pp. 21–23.

[6] W. A. Newcomb, Ann. Phys. **10**, 232 (1960).

[7] A. D. Miller and R. L. Dewar, J. Comput. Phys. **66**, 356 (1986).

[8] A. Pletzer and R. L. Dewar, J. Plasma Phys. **45**, 427 (1991).

[9] S. Tokuda, Private Communication, 1993.

[10] M. Abramowitz and I. Stegun, in *Handbook of Mathematical Functions* (Dover Publications, Inc., New York, 1972), p. 374.

[11] X. Llobet, K. Appert, A. Bondeson, and J. Vaclavik, Comput. Phys. Commun. **59**, 199 (1990).

[12] K. W. Morton, in *Finite Elements in Physics*, edited by R. Gruber (North-Holland, Amsterdam, 1987), p. 61.

[13] K. Appert, R. Gruber, and J. Vaclavik, Phys. Fluids **17**, 1471 (1974).

[14] A. Pletzer, A. Bondeson, and R. L. Dewar, J. Comput. Phys. **115**, 530 (1994).

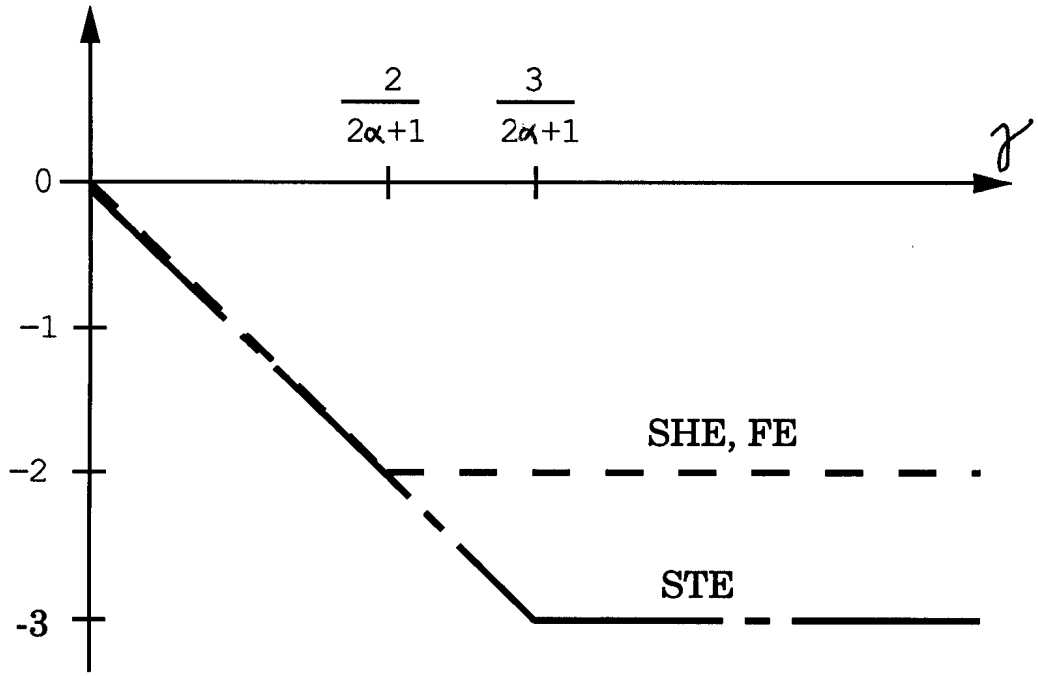

Fig. 1. Schematic representation of the energy W_{H} convergence rates versus the mesh node packing exponent γ for the SHE and STE schemes. The standard FE element scheme (FE) has the same convergence rate as the SHE scheme.

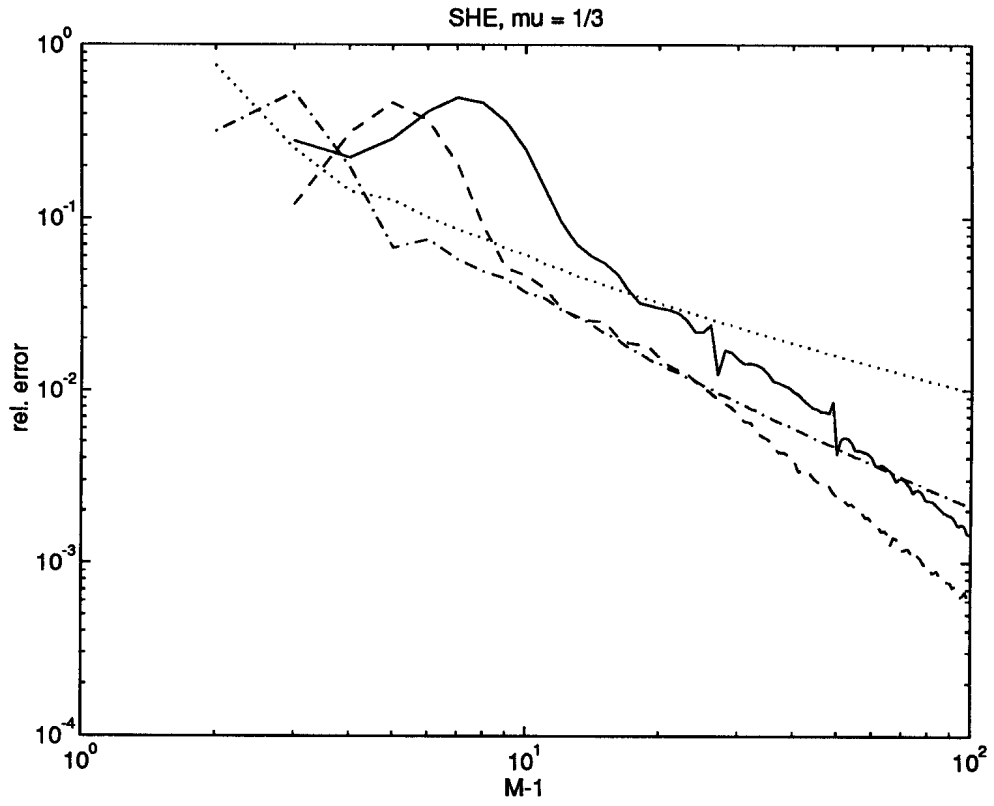

Fig. 2. Relative error in W_{H} of the SHE scheme for the case $\mu = 1/3$, versus the number $M - 1 = 2, 3, 4 \cdots 100$ of mesh intervals. Various mesh packing exponents: $\gamma = 1$ (dotted line), $\gamma = 1.5$ (dash-dotted line), $\gamma = 1.5$ (dashed line) and $\gamma = 4.5$ (solid line) have been used.

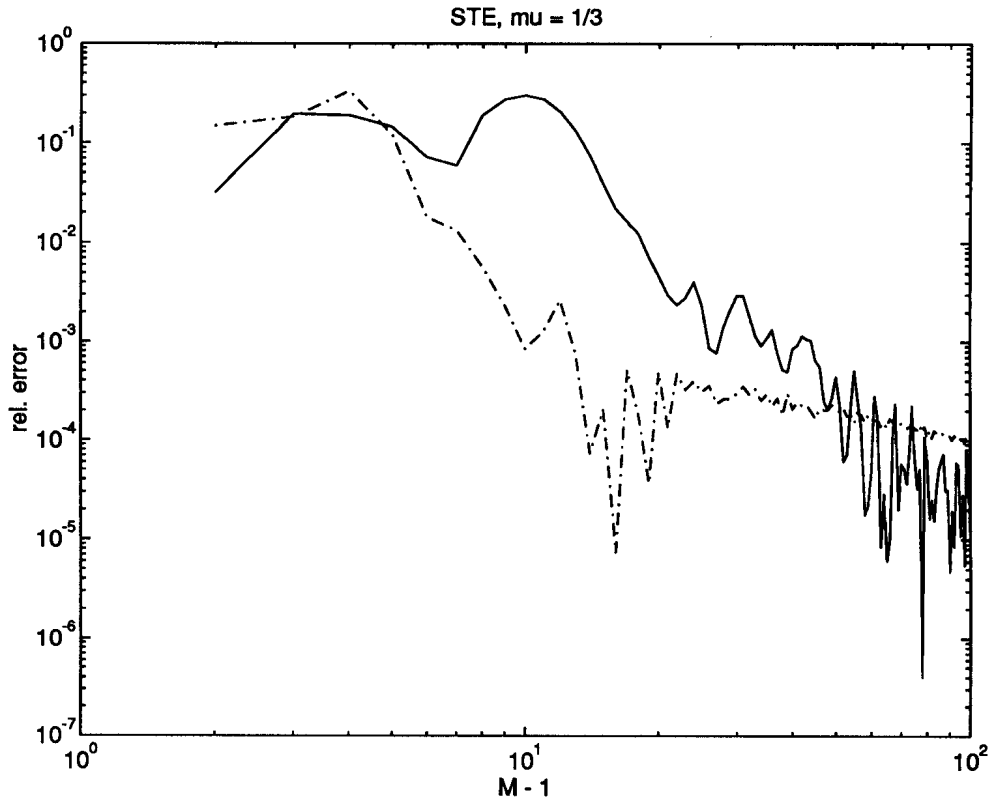

Fig. 3. Relative error in W_{H} of the STE scheme for the case $\mu = 1/3$, versus the number $M - 1 = 2, 3, 4 \cdots 100$ of mesh intervals. Two mesh packing exponents: $\gamma = 1.5$ (dash-dotted line) and $\gamma = 2.25$ (solid line) have been used.

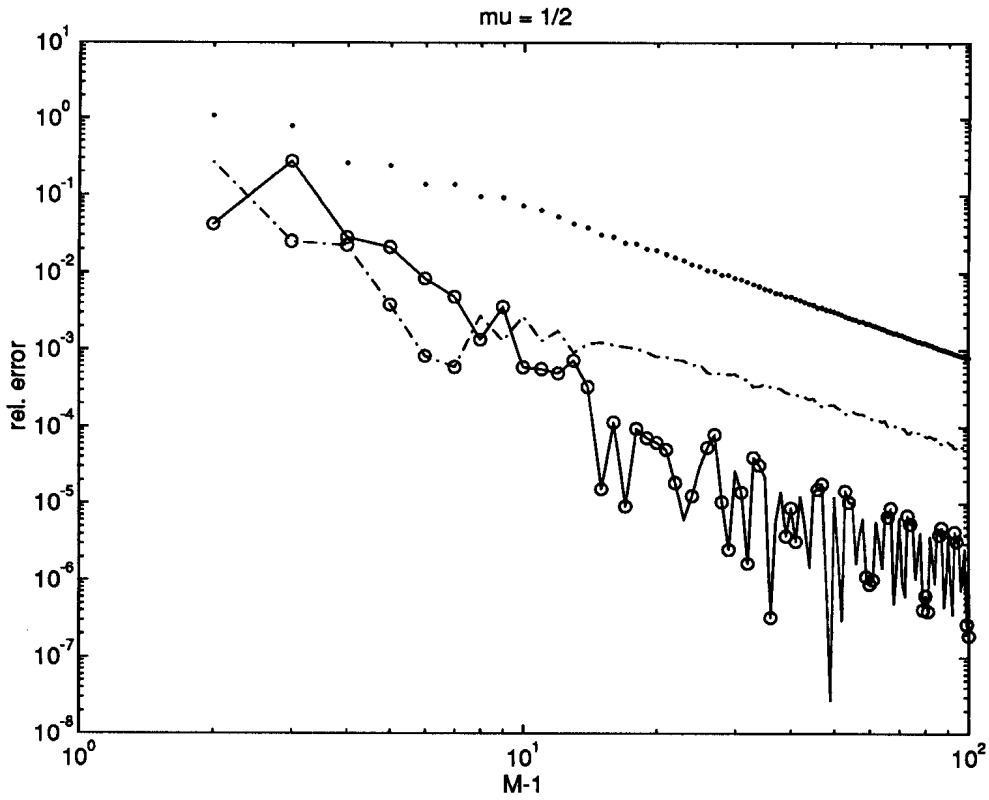

Fig. 4. Comparison of the error convergence of the SHE (dash-dotted line), STE (solid line) and the FE method (dotted line) for the case $\mu = 1/2$. A linear mesh has been adopted. The circles correspond to a negative error $W_{\mathrm{H}}(\epsilon, \epsilon)$.

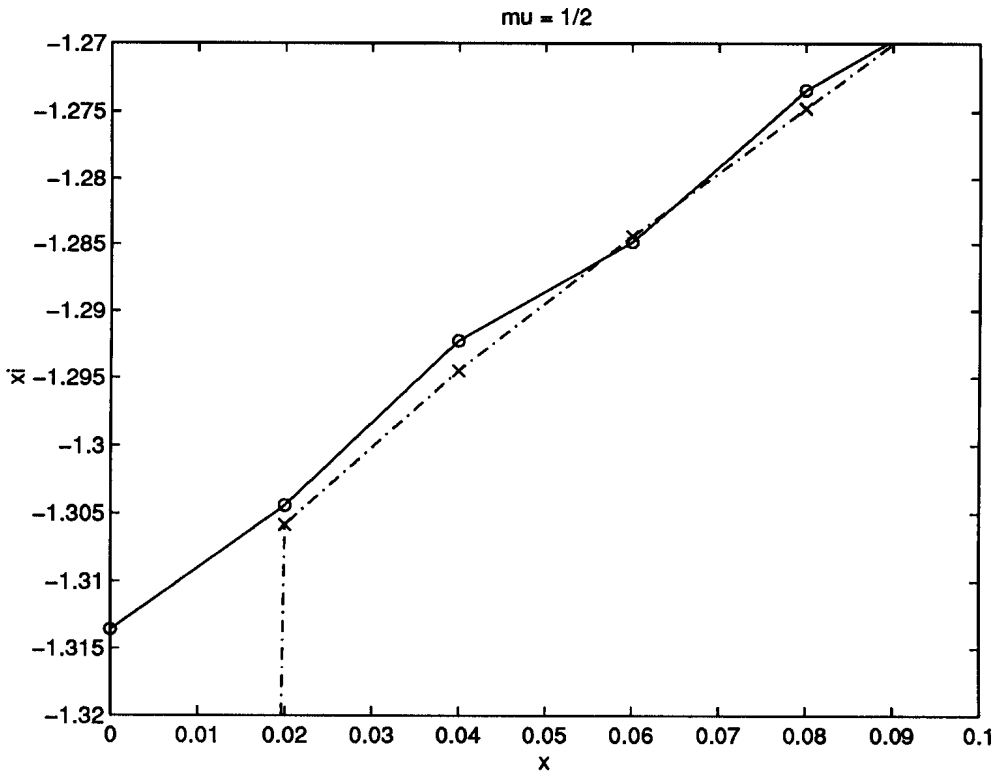

Fig. 5. Solution $\check{\xi}$ obtained using the STE (solid line) and the SHE (dash-dotted line) in the neighbourhood of $x = 0$ for $\mu = 1/2$ and $\Delta' = -1.3130352855$.

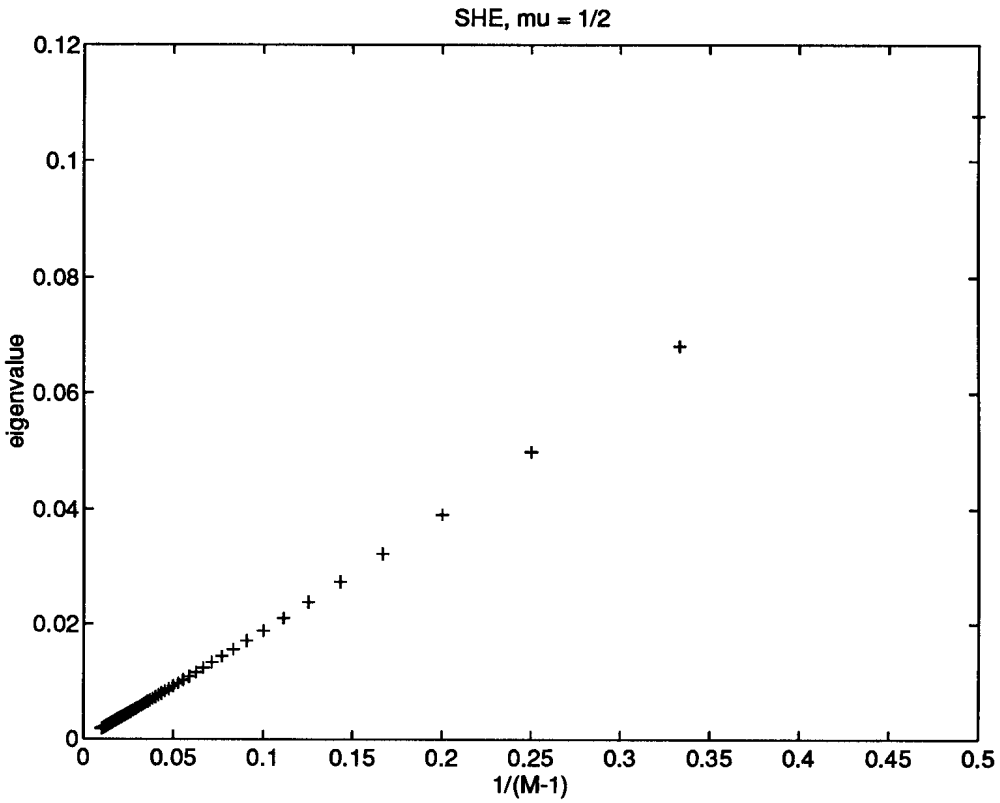

Fig. 6. Spurious eigenvalue of the STE scheme versus the inverse number of mesh node intervals.

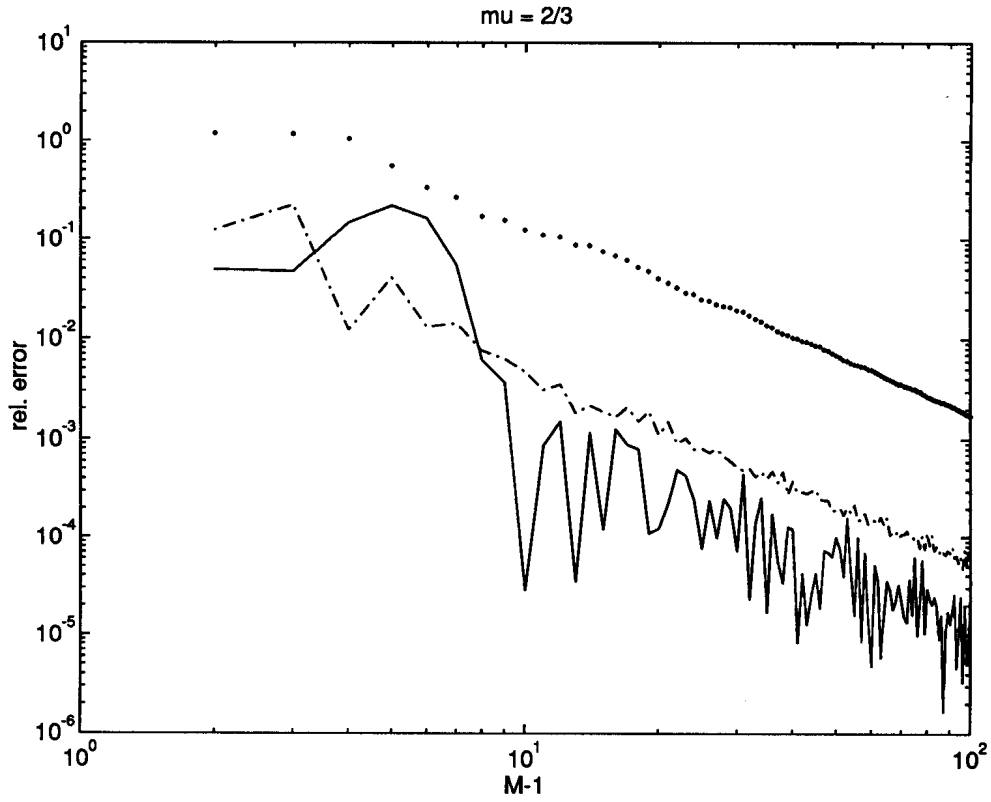

Fig. 7. Comparison of the error convergence of the SHE (dash-dotted line), STE (solid line) and the FE method (dotted line) for the case $\mu = 2/3$. A mesh packing exponent $\gamma = 1/\mu$ has been used for the SHE and FE methods, and $\gamma = 3/(2\mu)$ for the STE scheme.